JTTEE5 15:46-52
DOI: 10.1361/105996306X92587
1059-9630/$19.00 © ASM International

Peer Reviewed

Detection of Thermally Grown Oxides in Thermal Barrier Coatings by Nondestructive Evaluation

A. Fahr, B. Rogé, and J. Thornton

(Submitted November 25, 2004; in revised form February 10, 2005)

The thermal-barrier coatings (TBC) sprayed on hot-section components of aircraft turbine engines commonly consist of a partially stabilized zirconia top-coat and an intermediate bond-coat applied on the metallic substrate. The bond-coat is made of an aluminide alloy that at high engine temperatures forms thermally grown oxides (TGO). Although formation of a thin layer of aluminum oxide at the interface between the ceramic top-coat and the bond-coat has the beneficial effect of protecting the metallic substrate from hot gases, oxide formation at splat boundaries or pores within the bond-coat is a source of weakness. In this study, plasma-sprayed TBC specimens are manufactured from two types of bond-coat powders and exposed to elevated temperatures to form oxides at the ceramic-bond-coat boundary and within the bond-coat. The specimens are then tested using nondestructive evaluation (NDE) and destructive metallography and compared with the as-manufactured samples. The objective is to determine if NDE can identify the oxidation within the bond-coat and give indication of its severity. While ultrasonic testing can provide some indication of the degree of bond-coat oxidation, the eddy current (EC) technique clearly identifies severe oxide formation within the bond-coat. Imaging of the EC signals as the function of probe location provides information on the spatial variations in the degree of oxidation, and thereby identifies which components or areas are prone to premature damage.

Keywords eddy current testing, nondestructive evaluation (NDE), thermal barrier coating (TBC), thermally grown oxide (TGO), ultrasonic testing

1. Introduction

The hot-section components of aircraft engines such as blades, guide-vanes, and combustors are often coated with a thermal barrier coating (TBC) to protect them from high-temperature degradation to prolong their service life. An air plasma-sprayed TBC system consists of a bond-coat that is applied to the metallic surface and a porous ceramic top-coat that covers the bond-coat. The top-coat is usually partially stabilized zirconia (PSZ) that has a low thermal conductivity and high durability compared with other ceramics (Ref 1). A stabilizer such as yttria is added to avoid the phase transformation of the zirconia at elevated temperatures (Ref 2, 3). The bond-coat, which is a modified aluminide alloy such as MCrAlY (where M is Co, Fe, Ni, or a combination thereof), serves to protect the substrate from high temperatures and a corrosive engine environment. It also improves the bonding of the ceramic zirconia to the metallic substrate and can reduce the thermal expansion mismatch between the two different materials (Ref 4, 5).

Although failure of a plasma-sprayed TBC often occurs by spallation due to stresses in the ceramic or in the bond-coat, the thermally grown oxides (TGO) that develop in the bond-coat also contribute to the problem (Ref 4). The oxidation of a CoNiCrAlY bond-coat ideally should occur at the ceramic bond-coat interface to provide a protective oxide layer of a few microns in thickness. However, if the bond-coat powder is of poor quality and inhomogeneous, oxides could form at the splat boundaries or pores within the bond-coat and lead to accelerated spallation (Ref 6). Factors such as the service temperature, severity of thermal shocks, and thickness of the bond-coat also play a role (Ref 7-11). Therefore, simple nondestructive evaluation (NDE) methods are needed that can detect severe bond-coat oxidation during engine overhauls such that damage-prone parts can be screened out. In this paper, the results of the application of ultrasonic and EC NDE methods for the detection of oxides in thermal-spray TBC coatings typical of those used in aircraft engine components are presented.

2. Specimens

For this investigation, a set of specimens was manufactured using commercial equipment (METCO 9MB gun) (Sulzer Metco, Winterthur, Switzerland) and automatic spraying. In all specimens, the substrate was a 2 mm thick Hastelloy-X and the ceramic top-coat was a 0.2-0.3 mm yttria-stabilized zirconia (8 wt.% of yttria), but two different bond-coat powders were used. In specimens 95,003 and 95,005, a prealloyed NiCoCrAlY (23Co18Cr13Al0.2Y balance Ni wt.% of each element) powder was used that resulted in a more uniform bond-coat (thickness: 0.12-0.16 mm). These specimens are referred to as "good" specimens. The other set (95,006 and 95,008) were made of a

A. Fahr and **B. Rogé,** Institute for Aerospace Research, National Research Council of Canada, K1A 0R6, Ottawa, Ontario, Canada; **J. Thornton,** Air Vehicles Division, Defence Science and Technology Organisation, Melbourne, Victoria 3207, Australia. Contact e-mail: abbas.fahr@nrc-cnrc.gc.ca.

powder with 2.5Co17.5Cr5.5Al0.5Y_2O_3 balance Ni wt.% of each element that had a larger particle size distribution and a greater amount of segregation resulting in a less uniform coating and referred to as "poor" specimens. Specimens 95,003 and 95,006 were exposed to 1150 °C in air for 20 h with slow cooling to accelerate formation of oxides whereas specimens 95,005 and

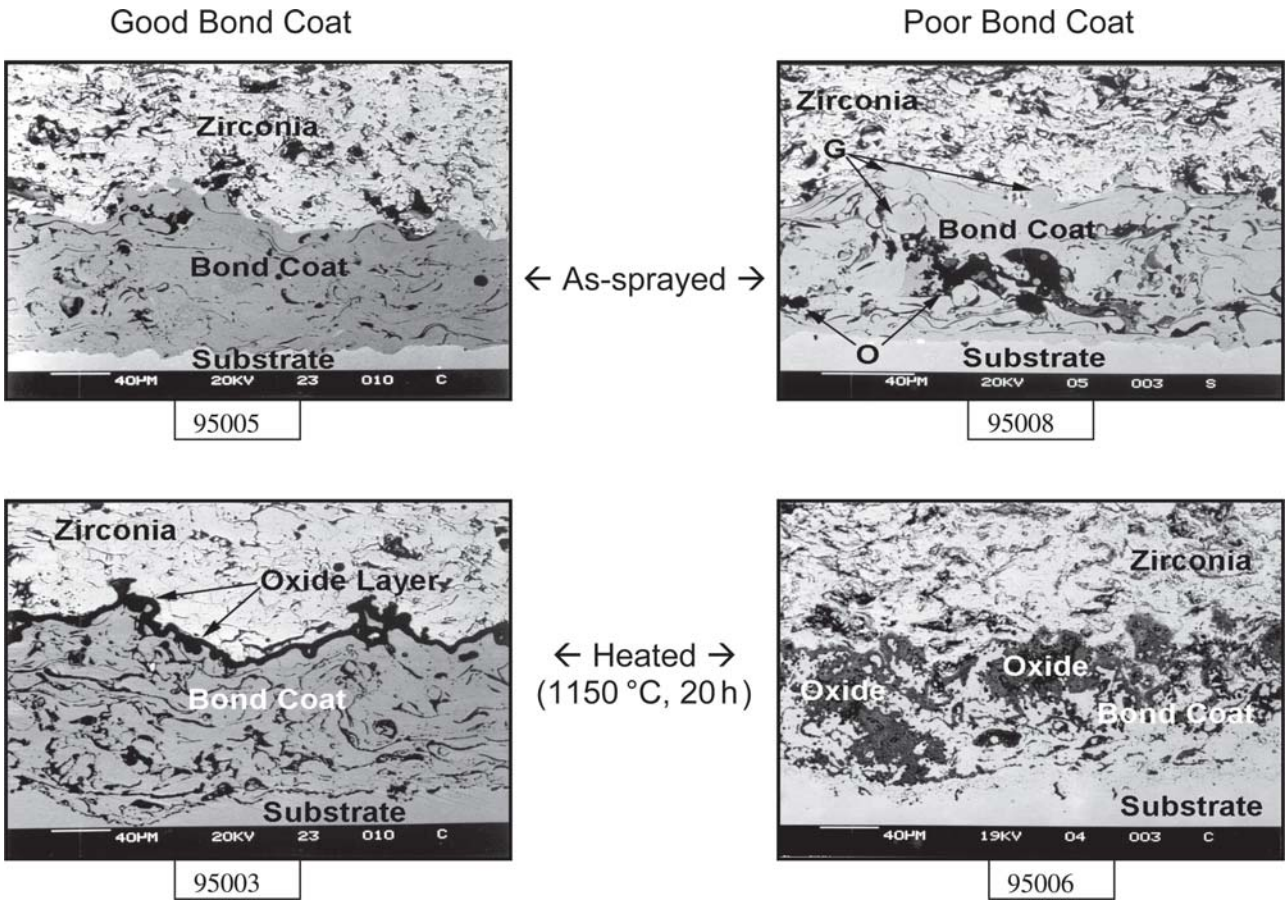

Fig. 1 Micrographs of the cross section of specimens with "good" and "poor" bond-coats in as-fabricated condition and after exposure to high temperature

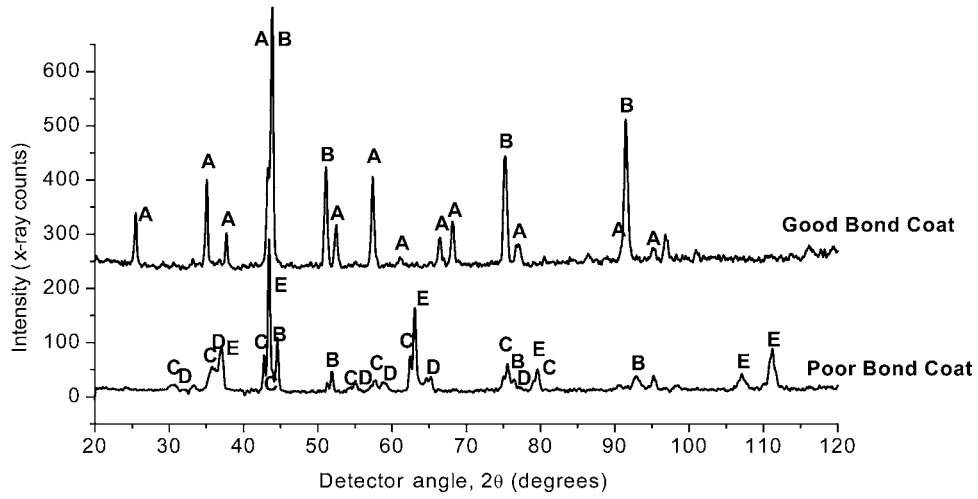

Fig. 2 XRD patterns from the good and poor bond-coat powders after exposure to elevated temperatures. The labels A-E refer to compounds identified in the XRD database (Ref 12). The good bond-coat pattern shows alumina (A: 42,1468 in Ref 12) and the bond-coat nickel alloy (B: nickel has pattern no. 4850 in Ref 12). The poor bond-coat also shows the bond-coat nickel alloy (B), and also nickel chromium oxide (C: 23,1272 in Ref 12), cobalt nickel oxide (D: 2,1074 in Ref 12), and nickel oxide (E: 44,1159 in Ref 12); however, no alumina was observed.

95,008 were kept in the as-fabricated condition. Figure 1 shows examples of the cross section of these specimens as seen under the microscope. These micrographs show formation of oxides in both heat-exposed specimens, however in the "good" specimens, the concentration of oxides was at the interface between the ceramic top-coat and the bond-coat whereas in the "poor" specimen a greater oxidation occurred in scattered form within the bond-coat. Nondestructive identification of the latter type of oxidation is of interest in this work. Figure 2 shows the x-ray diffraction (XRD) patterns (Ref 12) from the bond-coat powders also after exposure to 1150 °C in air for 20 h. Aluminium oxide was found on the "good" bond-coat powder but not on the "poor" bond-coat powder that had a low aluminium content. There, nickel oxide, nickel cobalt oxide, and nickel chromium oxide were found.

3. Ultrasonic Testing

Ultrasonic testing (UT) is based on the detection of ultrasonic reflections or the measurement of changes in velocity or attenuation and is widely used for flaw detection, material characterization, and component quality control. In this work, relative attenuation measurements were carried out by raster scanning of the specimens in a water tank using a 5-MHz probe placed at the normal angle with respect to the coated surface. Measurements

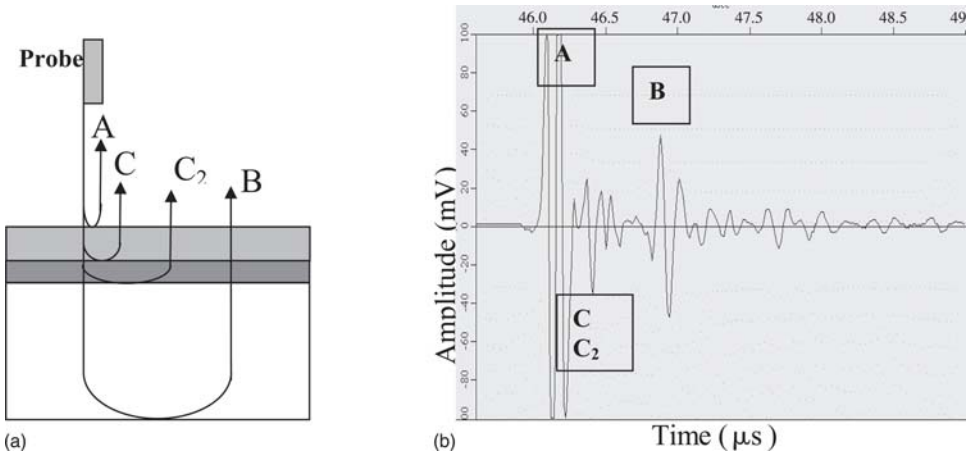

Fig. 3 (a) Ultrasonic pulse-echo test configuration and (b) a typical return signal from a TBC specimen (amplitude scale, 20 mV/division; time scale, 0.5 μs/division)

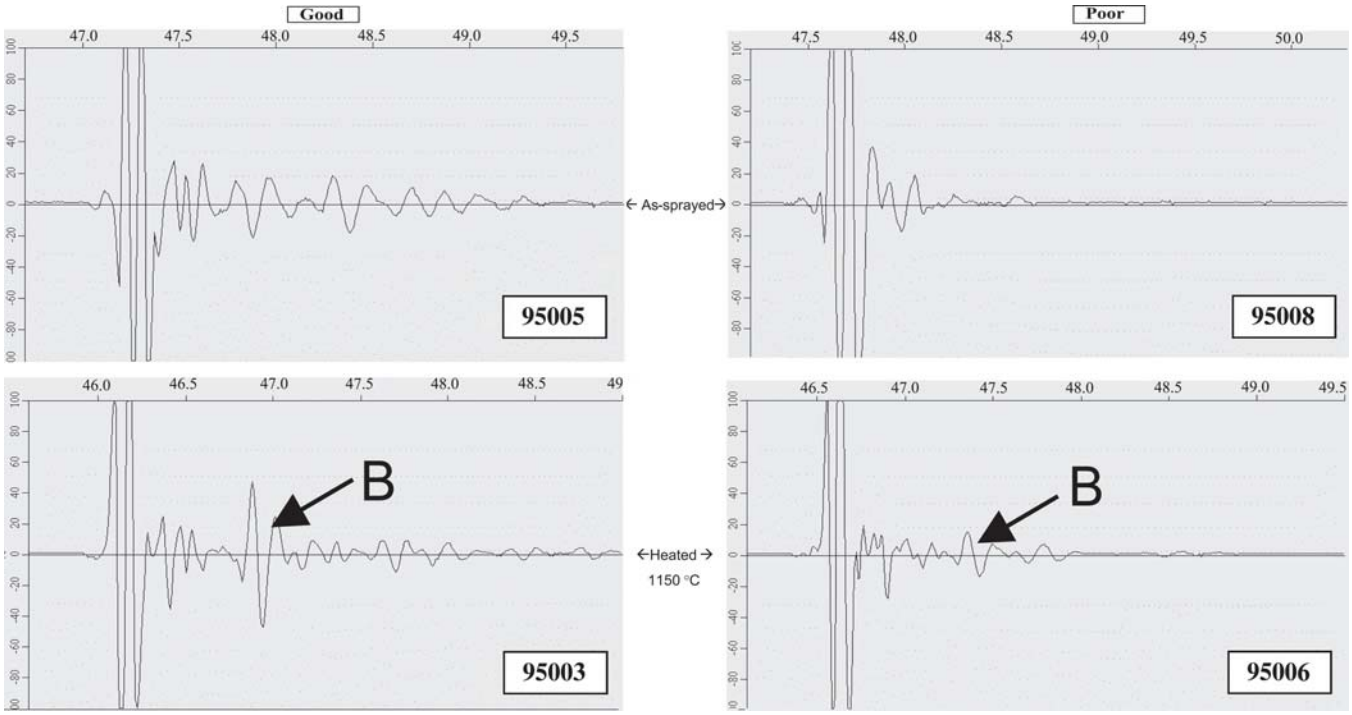

Fig. 4 Ultrasonic signals of the as-sprayed and heat-treated TBC specimens made with good and poor bond-coat powders. The gain is the same in all. B indicates the position of back-wall echo; amplitude scale: 20 mV/division; time scale: 0.5 μs/division

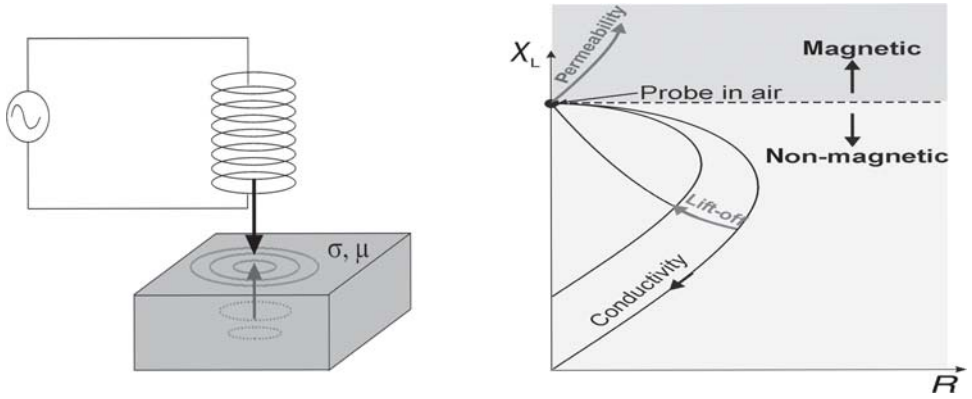

Fig. 5 EC test configuration and an impedance plane diagram

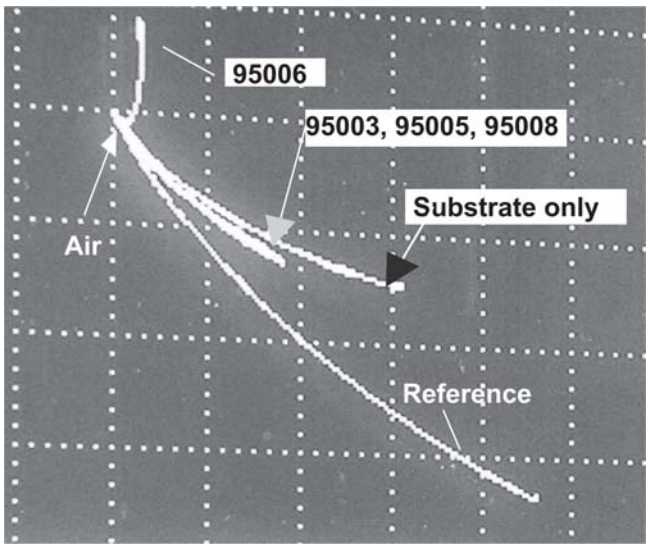

Fig. 6 EC signals taken from the coating side of specimens made with good and poor bond-coat powders compared with signals from substrate alone and copper (reference)

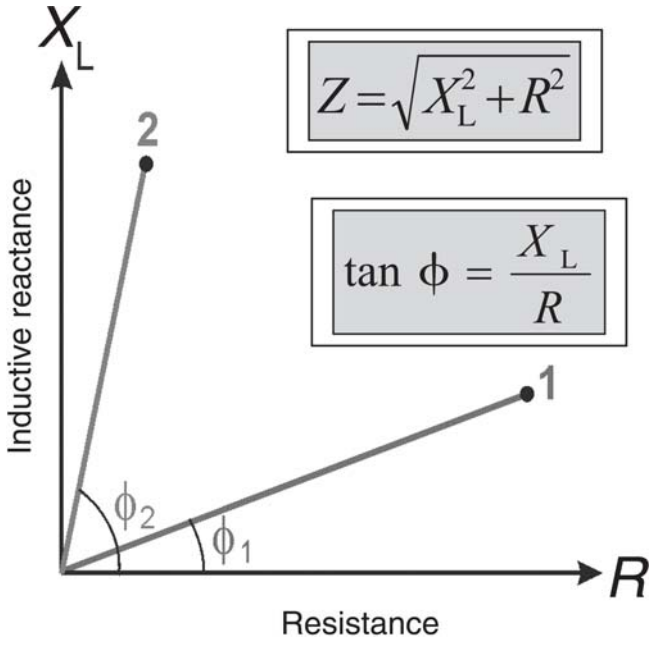

Fig. 7 Electromagnetic equations used in EC testing (schematic), showing the change in impedance between TBC with good (1) and a poor (2) bond-coats

were carried out using a commercial ultrasonic instrument (Panametrics 5601A/TT, Waltham, MA), a digitizer with a 500-MHz sampling frequency (Compuscope 8500, Gage Applied Technologies, Inc., Quebec, QC, Canada), and Winspect software (UTEX, Mississauga, ON, Canada). Figure 3 shows the ultrasonic pulse-echo test configuration used and a typical ultrasonic signal obtained at 5-MHz frequency. As seen in this figure, at 5-MHz frequency, due to the small thickness of the coating layer, echoes from the individual boundaries cannot be easily differentiated from each other or from the top-surface echo but the small echo corresponding to the substrate back wall is more visible. Higher frequencies could have been used to reduce signal overlap, but due to the high attenuation of the ceramic top-coat, this was not practical. At frequencies higher than 5 MHz, not only the echoes from the coating interfaces cannot be seen but also the back-wall echo disappears due to higher attenuation. Therefore, 5 MHz was found to be the optimal frequency for the specimen types investigated here.

The UT signals taken from the center of the four different specimens, shown in Fig. 4, indicate some differences. First, the substrate back-wall echo is more visible in specimens made out of a good bond-coat powder. The weaker echoes in the poor bond-coat specimen indicate higher acoustic attenuation in these specimens associated with the larger and less uniform bond-coat particle sizes. Second, the heat-exposed specimens produced stronger substrate back-wall echoes than the as-manufactured ones indicating that the formation of oxides actually improves acoustic transmission. This may be due to the fact that oxides form at grain boundaries and within pores filling minute air gaps that cause attenuation. To observe materials flaws by NDE, automated raster scanning and imaging (C-scan) is often used by mapping a parameter of the NDE signal as the function of the probe location on the test piece. Ultrasonic amplitude C-scans indicated that, despite the differences in the signals, imaging of the scattered oxidation was not possible due to the slight curva-

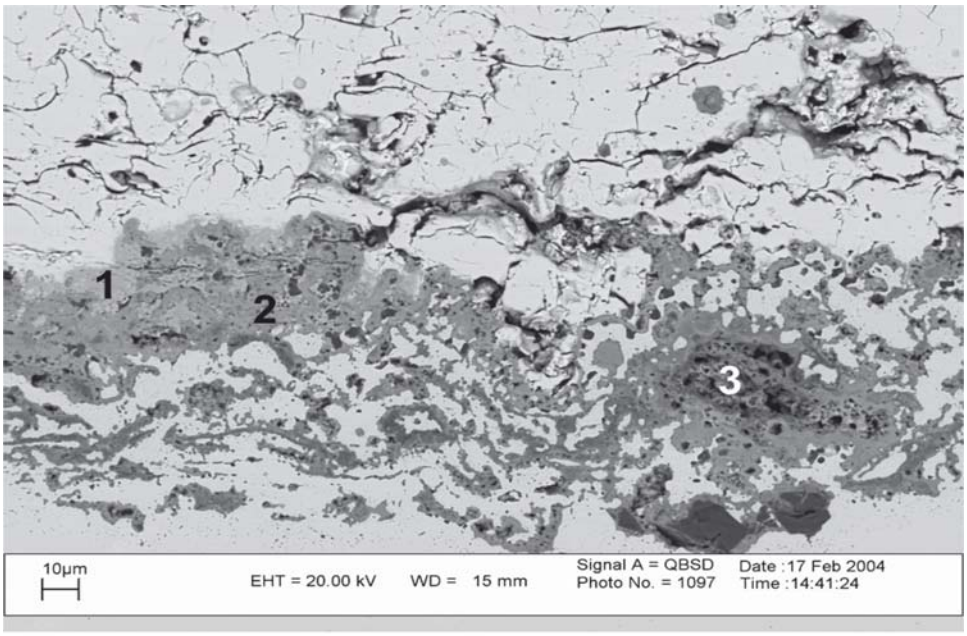

Element	Position 1	Position 2	Position 3
O	52.2	55.7	56.4
Al		2.3	19.6
Co	1.6	1.6	6.5
Cr	0.8	20.6	9.6
Fe	1.7	4.4	0.2
Ni	42	15.4	7.6
Zr	1.7		
Mo			0.1

Fig. 8 SEM micrograph of the bond-coat region of severely oxidized specimen (95,006) and the x-ray spectroscopy data showing atomic percent of elements at positions shown in the image

ture of the specimens that degraded C-scan images. For this reason and the fact that the C-scan method requires immersion of parts in a water bath, ultrasonic C-scan testing of complex TBC engine components is not practical, especially in industrial environments.

4. Eddy Current Testing

Eddy current (EC) testing is based on the principles of electromagnetic induction and is sensitive to the electrical conductivity and magnetic permeability of conductive materials. The EC technique does not require direct electrical contact; rather, a coil probe is placed adjacent to the part being inspected. An alternating electrical current at one or a few discrete frequencies is applied to the coil to induce an EC in the test medium. This induced current in turn creates a secondary field that is picked up by the coil and displayed in the form of an impedance plane diagram. Figure 5 shows the EC test principles and an EC impedance plane (the horizontal axis is resistance, and the vertical axis is inductive reactance). Most commercial instruments use a single point on the impedance plane to display the EC sinusoid signal. In the simplest case, the response of the probe alone (air point) is considered as the zero point, and changes in the position of this point when the probe is placed on the test material are measured in terms of its distance to zero point (amplitude) and its angle with respect to the horizontal axis (phase).

EC NDE is applicable to both magnetic and nonmagnetic materials; however, when the permeability of nonmagnetic materials is equal to 1, magnetic materials exhibit different levels of natural permeability (Ref 14, 15).

In this work, tests were carried out using a ZETEC MIZ-40A instrument (ZETEC, Issaquah, WA) along with an EC-NDT LLC PAUM0040 probe (Federal Way, WA) that has an operating frequency range of 50-500 kHz. The EC response of the specimens was obtained at 250 kHz both from the substrate side as well as the coating side by plotting the impedance plane response when the probe is moved from air onto the surface. As seen in Fig. 6, when EC tests were carried out from the coating side, all specimens showed similar response except for specimen

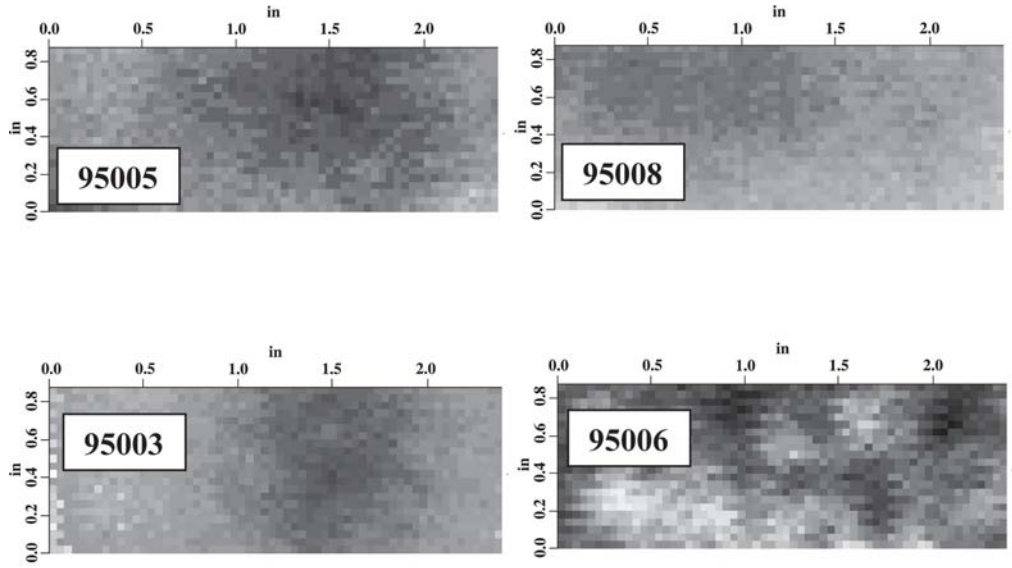

Fig. 9 EC C-scan images of the different TBC specimens: 95,005, as-sprayed good bond-coat; 95,008, as-sprayed poor bond-coat; 95,003, heated good bond-coat; and 95,006, heated poor bond-coat

95,006, which is made of a poor bond-coat powder that has formed extensive oxidation within the bond-coat during high-temperature exposure.

To explain the EC results, the electrical and magnetic characteristics of the main substances of the TBC system were evaluated using simple equations used in EC testing, as shown in Fig. 7 (Ref 13, 14).

In the TBC samples investigated, the Hastelloy X substrate is a nickel-based metal, which is a conductive and nonmagnetic material. The conductivity of the Hastelloy X substrate was measured directly before and after exposure to high temperatures using a digital conductivity meter (Hocking Auto-Sigma 2000, St Albans, England) and a commercial 250-kHz EC pencil probe. It was found that the conductivity of the substrate remains unchanged at 1.35% IACS (International Annealed Copper Standard). Based on the information in the open literature (e.g. www.suppliersonline.com), the Hastelloy X substrate is a nonmagnetic alloy with a magnetic permeability of 1.002. Thus, the influence of the substrate on the EC response under identical test conditions is the same for all specimens. This was also confirmed by taking direct EC measurements on the substrate alone.

The ceramic zirconia top-coat is nonconductive and nonmagnetic (Ref 15) and therefore behaves like an air gap between the EC probe and the conductive substrate and only creates a probe lift-off effect. Because the zirconia thickness is the same in all specimens, the lift-off remains unchanged and therefore the influence of the top-coat on the EC signal also remains unchanged.

The bond-coat before formation of oxides is conductive and its influence on the EC response is similar to the substrate. However, after formation of oxides, its electromagnetic characteristics changes. X-ray spectroscopy was used to identify the nature of oxides formed in the bond-coat and the results are shown in Fig. 8. Except for aluminum oxide and zirconium oxide, which are nonmagnetic (Ref 15), all the other oxides formed in the bond-coat, particularly nickel oxide, chromium oxide, and iron oxide, have a magnetic permeability >1 (Ref 15). Using the simple equations shown in Fig. 7, the combined effect of the formation of large quantities of magnetic oxides on the EC data would be an increase in the EC phase angle. Repeated tests on various locations of the same specimens by different inspectors using conventional EC at different frequencies as well as pulsed EC confirmed the results showing increased phase angle in the severely oxidized specimen. In fact, simple tests with a permanent magnet also showed that the severely oxidized "poor" specimen is more magnetic than the "good" ones. Thus, simple EC phase angle measurements appear to have the potential to detect the formation of magnetic oxides due to severe oxidation of the bond-coat. Further tests on a larger number of specimens with different degrees of oxidation are needed to establish the accuracy of the results and also the correlation between the amount of oxides and the resulting EC response. Such tests have been planned for the future. EC modeling would also be helpful in predicting the EC response of specific TBC systems before and after oxidation, and such analysis is underway.

To observe severely oxidized sites, once again C-scan imaging was used by scanning the specimens in an automated *x-y* scanner equipped with the above-mentioned EC equipment and data acquisition and analysis software (Wispect, UTEX, Mississauga, ON, Canada). Tests were performed from the coating side of the samples on which a Teflon tape was adhered to protect the EC probe from wearing out. The resulting 2-dimensional images of the phase angle are presented in Fig. 9. Once again only specimen 95,006, which has a larger amount of oxidation, showed scattered darker areas that are associated with oxide agglomerates.

5. Conclusions

The potential of ultrasonic and EC techniques for the detection of oxide formation in thermal barrier coatings has been stud-

ied. While the ultrasonic technique is useful in the laboratory environment to study the formation of oxides in simple and flat TBC specimens, it requires immersion in water, and its use on actual engine parts will be very limited. On the other hand, the EC technique is nonintrusive and relatively easy to apply on simple or complex parts; however, interpretation of results requires considerable knowledge of the electromagnetic properties of the test object as well as the technique itself. This study showed that the formation of magnetic oxides in TBC bond-coat due to exposure to elevated temperatures affects the EC phase angle depending on the location and extent of oxidation. While formation of a thin layer of oxides at the interface of zirconia and the bond-coat is acceptable and does not change the EC signature, extensive oxidation of the bond-coat, which is undesirable, affects the EC response by increasing the phase angle. Thus EC phase angle measurement appears to have the potential to detect magnetic oxides in the bond-coat and help to prevent severely oxidized parts from re-entering into service.

Acknowledgments

This work was carried out between Canada and Australia under the auspices of The Technical Cooperation Program (TTCP) technical panel MAT-TP-5, with financial support from the National Research Council Canada, the Canadian Department of National Defence, and the Defence Science and Technology Organisation of Australia. The authors thank Dr. Steve Burke of DSTO and Dr. Catalin Mandache of NRC for their technical contributions.

References

1. T.M. Yonushonis, R.J. Stafford, T. Ahmed, L.D. Favro, P.K. Kuo, and R.L. Thomas, Thermal Wave Imaging of Thermal Barrier Coatings for Diesel Applications, *Am. Ceram. Soc. Bull.,* 1992, 71 (8), p 1191-1202
2. P.D. Harmsworth and R. Stevens, Phase Composition and Properties of Plasma-Sprayed Zirconia Thermal Barrier Coatings, *J. Mater. Sci.,* 1992, 27, p 611-615
3. O. Knotek, F. Loffler, and W. Beele, Diffusion Barrier Design Against Rapid Interdiffusion of MCrAlY and Ni-Base Material, *Surf. Coat. Technol.,* 1993, 61, p 6-13
4. R.A. Miller, Current Status of Thermal Barrier Coatings—An Overview, *Surf. Coat. Technol.,* 1987, 30, p 1-11
5. J. Wigren and L. Pejryd, Thermal Barrier Coatings: Why, How, Where and Where To, *Proceedings of the 15th International Thermal Spray Conference,* Nice, France, 25-29 May 1998, ASM International, p 1531-1542
6. J. Thornton, N. Ryan, and G. Stocks, The Production of Stresses in Thermal Barrier Coating Systems by High Temperature Oxidation, *Proceedings of the National Thermal Spray Conference: Thermal Spray Industrial Applications,* Boston, MA, C.C. Berndt and S. Sampath, Ed., ASM International, 1994, p 633-636
7. L. Lelait, S. Alperine, C. Diot, and M. Mevrel, Thermal Barrier Coatings: Microstructural Investigation after Annealing, *Mater. Sci. Eng. A,* 1989, 121, p 475-482
8. L. Lelait, S. Alperine, and R. Mevrel, Alumina Scale Growth at Zirconia-MCrAlY Interface: A Microstructural Study, *J. Mater. Sci.,* 1992, 7, p 5-12
9. Z.A. Chaudhury, G.M. Newaz, S.Q. Nusier, T. Ahmed, and R.L. Thomas, Chronological Evaluation of Interface Damage in TBC Due to Thermal Cycling, *J. Mater. Sci.,* 1999, 34, p 2475-2481
10. Z.A. Chaudhury, G.M. Newaz, and T. Ahmed, Interfacial Cracking Due to Isothermal Heating in Thermal Barrier Coatings (TBCs), *J. Mater. Sci. Lett.,* 1998, 17, p 85-87
11. A.C. Léger, J. Wigren, and M.O. Hansson, Development of a Process Window for a NiCoCrAlY Plasma-Sprayed Coating, *Surf. Coat. Technol.,* 1998, 108-109, p 86-92
12. International Centre for Diffraction Data, ICDD-JCPDS Database of Crystallographic data, 12 Campus Blvd., Newtown Square, Pennsylvania
13. *Non-Destructive Testing Handbook*, Electromagnetic Testing, Vol 4, 2nd ed., ASNT, Columbus, Ohio, 1986
14. *Handbook of Chemistry and Physics,* 83rd ed., CRC Press, LLC, Boca Raton, Florida, 2002-2003
15. Magnetic Properties and Susceptibilities Chart, www.reade.com/Particle_Briefings/magnetic_susceptibilities.html (November 2004)